C–Cl bond fission dynamics and angular momentum recoupling in the 235 nm photodissociation of allyl chloride

Yi Liu and Laurie J. Butler
James Franck Institute and Department of Chemistry, The University of Chicago, Chicago, Illinois 60637

(Received 24 June 2004; accepted 14 September 2004)

The photodissociation dynamics of allyl chloride at 235 nm producing atomic $Cl(^2P_J; J=1/2,3/2)$ fragments is investigated using a two-dimensional photofragment velocity ion imaging technique. Detection of the $Cl(^2P_{1/2})$ and $Cl(^2P_{3/2})$ products by [2+1] resonance enhanced multiphoton ionization shows that primary C–Cl bond fission of allyl chloride generates 66.8% $Cl(^2P_{3/2})$ and 33.2% $Cl(^2P_{1/2})$. The $Cl(^2P_{3/2})$ fragments evidenced a bimodal translational energy distribution with a relative weight of low kinetic energy $Cl(^2P_{3/2})$/high kinetic energy $Cl(^2P_{3/2})$ of 0.097/0.903. The minor dissociation channel for C–Cl bond fission, producing low kinetic energy chlorine atoms, formed only chlorine atoms in the $Cl(^2P_{3/2})$ spin–orbit state. The dominant C–Cl bond fission channel, attributed to an electronic predissociation that results in high kinetic energy Cl atoms, produced both $Cl(^2P_{1/2})$ and $Cl(^2P_{3/2})$ atomic fragments. The relative branching for this dissociation channel is $Cl(^2P_{1/2})/[Cl(^2P_{1/2})+Cl(^2P_{3/2})]=35.5\%$. The average fraction of available energy imparted into product recoil for the high kinetic energy products was found to be 59%, in qualitative agreement with that predicted by a rigid radical impulsive model. Both the spin–orbit ground and excited chlorine atom angular distributions were close to isotropic. We compare the observed $Cl(^2P_{1/2})/[Cl(^2P_{1/2})+Cl(^2P_{3/2})]$ ratio produced in the electronic predissociation channel of allyl chloride with a prior study of the chlorine atom spin–orbit states produced from HCl photodissociation, concluding that angular momentum recoupling in the exit channel at long interatomic distance determines the chlorine atom spin–orbit branching. © *2004 American Institute of Physics.* [DOI: 10.1063/1.1812757]

I. INTRODUCTION

Alkyl and alkenyl halides have played an important role in the understanding of photodissociation dynamics of polyatomic organic molecules. They are also convenient precursors for the generation of specific hydrocarbon radical isomers.[1–3] After excitation by a UV photon, either carbon-halogen bond fission or molecular hydrogen halide elimination can occur. The mechanism for the carbon-halogen fission channel includes a competition between internal conversion to high vibrational levels of the electronic ground state and a mechanism involving curve crossing from the initially accessed electronic excited state to a state repulsive along the carbon–halogen bond. The latter produces high kinetic energy halogen atoms, while the former generates low kinetic energy halogen atoms. Measuring the angular and velocity distributions as well as the spin–orbit branching ratios for the atomic halogen fragments serves as a powerful probe of the dissociation dynamics. Lab velocity distributions for the atomic fragments determine the internal energy distributions of the nascent radical cofragments and can probe the character of the dissociative states and the interactions in the exit channels. Angular distributions can provide information about the ground-state conformation and the symmetry and lifetime of the parent dissociative excited states.

Previous photofragment translational spectroscopy experiments in our group on the photodissociation of allyl chloride at 193 nm have identified two C–Cl bond fission pathways.[2,3] C–Cl fission that released a large fraction of the total available energy into product recoil was attributed to a mechanism involving predissociation via a singlet $n\sigma^*$ repulsive state after excitation to the dominant $\pi\pi^*$ state (with some admixture of $n\sigma^*$ character in the adiabatic electronic configuration in the Franck–Condon region). Internal conversion from the initially excited $\pi\pi^*$ state to the vibrationally excited ground state was proposed to be responsible for the minor C–Cl fission channel. The angular distribution of the recoiling chlorine fragments was also measured to be slightly anisotropic, and perpendicular in character. The spin–orbit fine structure states of the chlorine products could not be distinguished in those experiments due to the limited selectivity of electron bombardment ionization and tunable vacuum ultraviolet photoionization detection.

In this study we employ the two-dimensional photofragment velocity-map imaging technique to investigate the primary C–Cl bond fission dynamics of allyl chloride at 235 nm. Using [2+1] resonance-enhanced multiphoton ionization (REMPI), we state selectively ionize the $Cl(^2P_{3/2})$ and $Cl(^2P_{1/2})$ fragments. The translational energy distributions and recoil anisotropies of the photoproducts are extracted from the ion images. The spin–orbit branching ratio between the two spin–orbit states is also determined. Results from this study qualitatively agree with our previous studies at 193 nm but are significantly different from those obtained in a prior study by Park, Lee, and Jung,[4] where they utilized similar methodology and the same wavelengths as ours to disso-

ciate allyl chloride and to probe the Cl atom photofragments. Three allyl chloride excited state predissociation channels producing $Cl(^2P_J; J=1/2,3/2)$ were proposed in their study, with the low-kinetic energy component attributed to internal conversion from the $\pi\pi^*$ state to the vibrationally hot ground state and the medium and high-kinetic energy components produced via curve crossings between the bound $\pi\pi^*$ state and the dissociative $\pi\sigma^*$ and $^1n\sigma^*$ states, respectively. The angular distributions were observed to be almost isotropic and the spin–orbit fine-structure branching ratio $Cl(^2P_{1/2})/Cl(^2P_{3/2})$ was determined to be 0.50.

II. EXPERIMENT

The experimental apparatus used in this work has been described previously.[5–7] The molecular beam is formed by expanding 500 Torr of helium containing about 10% allyl chloride vapor (allyl chloride is purchased from Aldrich with a stated purity 99%, and used without further purification) through a pulsed valve (General Valve) with 0.6 mm orifice which is typically driven by a voltage pulse (220–350 μs, 20 Hz). The operation of the valve is synchronized with the laser pulses. After passing through a skimmer located ~20 mm downstream from the nozzle, the molecular beam travels another 51 mm to the center of the reaction chamber. The main chamber base pressure is 4×10^{-8} Torr. The 532 nm output of a Nd:YAG (yttrium aluminum garnet) laser (Continuum) is used to pump a dye laser (Lambda Physik, FL3002, LDS698 dye) which generates visible radiation in the region of 675–715 nm. The dye laser output is frequency doubled in a potassium dihydrogen phosphate crystal and the resulting 353 nm light is mixed with the 706 nm fundamental in a BBO (β-barium borate) crystal to produce the 235 nm UV radiation. The 235 nm light is linearly polarized along an axis vertically perpendicular to the molecular beam and parallel to the detector surface. The power is reduced to ~1.25 mJ/pulse to minimize Coulomb repulsion between the ions formed in the interaction region. A focusing lens (10″ focal length) is inserted in front of the main chamber window to focus the laser light into the reaction region.

In a one-color experiment, parent molecules are dissociated by the 235 nm laser and the $Cl(^2P_{1/2})$ and $Cl(^2P_{3/2})$ fragments are ionized via [2+1] REMPI at 235.20 nm ($4p\,^2P_{1/2}\leftarrow3p\,^2P_{1/2}$) and 235.34 nm ($4p\,^2D_{3/2}\leftarrow3p\,^2P_{3/2}$), respectively.[8] The spherically expanding $Cl(^2P_{1/2})/Cl(^2P_{3/2})$ ion clouds are then accelerated toward a two-dimensional position-sensitive detector by an electrical ion lens assembly[6] with a repeller voltage of 2000 V and extractor voltage of 1424 V. After flowing through the ~577 mm time-of-flight drift region, the ions strike the detector (Burle 3040FM) which consists of a chevron multichannel plate (MCP) coupled with a $P20$ phosphor screen by fiber optics. In order to detect only the ions of interest, the front plate of the MCP is pulsed to −500 V at the appropriate arrival time with a pulse width of 150 ns. The phosphor screen is maintained at 2.5 kV above the potential of the rear MCP plate. Images appearing on the phosphor screen are recorded by a 1376 ×1040 pixel charge-coupled device camera (LaVision Imager 5) with a standard 35 mm camera lens (Nikon). Each image is constructed by accumulating signals from ≈6000 laser shots, and scanning the laser wavelength over the entire Doppler profile of the detected species. Background counts generated by the laser light alone (molecular beam off) are subtracted.

III. RESULTS AND ANALYSIS

This experiment investigates the C–Cl bond fission channels of allyl chloride at 235 nm photodissociation, resolving the branching between the $Cl(^2P_{1/2})$ and $Cl(^2P_{3/2})$ products for both the high-kinetic energy and the low-kinetic energy dissociation channels using [2+1] REMPI detection. The G3//B3LYP bond energy is 68.0 kcal/mol,[9] so the energy available to partition into product recoil translational energy and internal energy of the nascent product allyl radical and chlorine atom spin–orbit energy is 53.5 kcal/mol (neglecting the small initial vibrational energy of the parent molecule). As the experiment is a one-color process, the photolysis wavelength changes slightly with the spin–orbit state of the chlorine atoms probed. The detection of $Cl(^2P_{3/2})$ and $Cl(^2P_{1/2})$ products using several REMPI lines in this region indicates that both the translational energy and the angular distributions are insensitive to the particular photolysis wavelength, confirming that the photodissociation dynamics does not change dramatically with wavelength over this narrow range. A power study on the production of the Cl fragment qualitatively confirmed that photodissociation of allyl chloride at 235 nm is a one-photon process.

A. Translational energy distributions

Raw images of the $Cl(^2P_{3/2})$ and $Cl(^2P_{1/2})$ photofragments are shown in Fig. 1 with the laser polarization direction in the vertical axis. The $Cl(^2P_{1/2})$ image displays only a high recoil kinetic energy channel, while the $Cl(^2P_{3/2})$ image shows two velocity components of the Cl atom product, with an intense high-kinetic energy component resembling that of the $Cl(^2P_{1/2})$ image and some low-kinetic energy signal distributed close to the center. The images have been reconstructed to three-dimensional scattering distributions using the Gaussian basis-set expansion Abel transformation method developed by Dribinski *et al.*[10] The speed distributions of the $Cl(^2P_J; J=1/2,3/2)$ products are extracted by integrating the three-dimensional speed distributions over all solid angles at each speed and the total center-of-mass translational energy distributions, $P(E_T)$'s, are derived from the $Cl(^2P_J; J=1/2,3/2)$ atom speed distributions using conservation of momentum and correcting for the appropriate Jacobian. The results are presented in Fig. 2. The allyl $+Cl(^2P_{1/2})$ translational energy distribution [Fig. 2(b)], showing only a single fast component, can be well characterized by a Gaussian function peaking at 30.2 kcal/mol with a full width at half maximum (FWHM) of 8.6 kcal/mol. The bimodal translational energy distribution based on the allyl $+Cl(^2P_{3/2})$ product can also be fit by two Gaussian functions [Fig. 2(a)]. The high-translational energy part peaks at 30.0 kcal/mol and the broad low-kinetic energy component is centered at 5.9 kcal/mol. The fractions for the high- and low-translational energy components in the $Cl(^2P_{3/2})$ data are

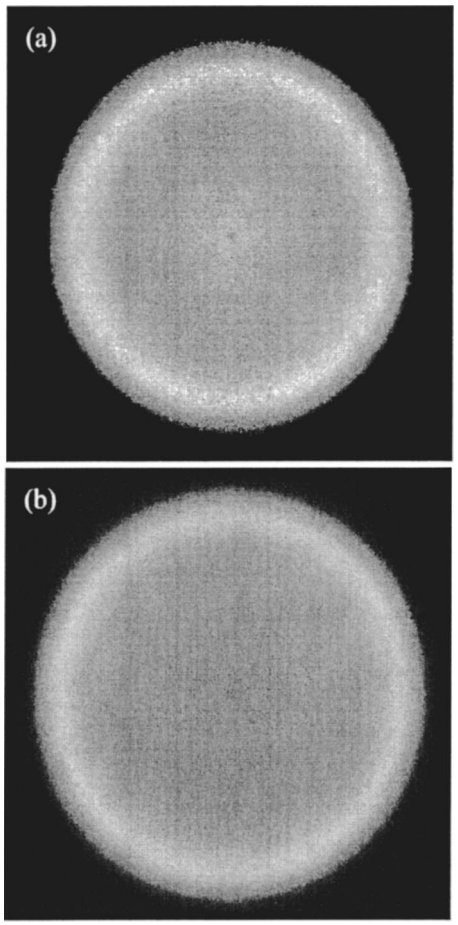

FIG. 1. Raw images of (a) $Cl(^2P_{3/2})$ obtained with dissociation and probe at 235.336 nm via the $4p\ ^2D_{3/2}\leftarrow 3p\ ^2P_{3/2}$ transition; (b) $Cl(^2P_{1/2})$ obtained with dissociation and probe at 235.205 nm via the $4p\ ^2P_{1/2}\leftarrow 3p\ ^2P_{1/2}$ transition. The laser polarization is along the vertical direction in the plane of the images. Each image consists of 861×861 pixels and is constructed by accumulating signals from ≈6000 laser shots. The distance of 1 cm on the phosphor screen corresponds to the width of 221.6 pixels in the images and 1310 m/s Cl atom recoil velocity.

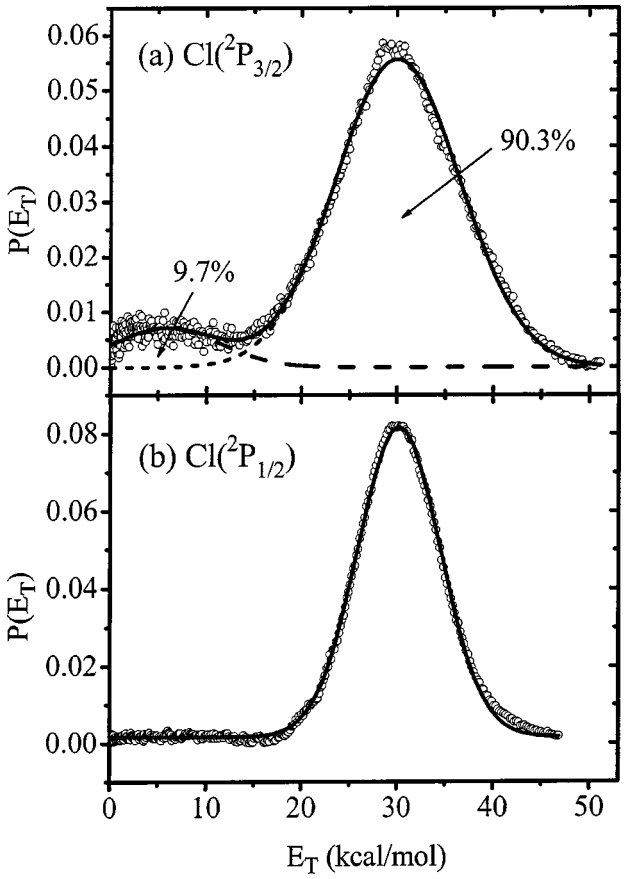

FIG. 2. Allyl+$Cl(^2P_J;J=1/2,3/2)$ center-of-mass translational energy distributions derived from Fig. 1: (a) allyl+$Cl(^2P_{3/2})$; (b) allyl+$Cl(^2P_{1/2})$. The distribution derived from the experimental data are shown in open circles; the solid lines show full fits to the translational energy distributions and the dashed lines indicate the Gaussian fits to the low- and high-kinetic energy components of $Cl(^2P_{3/2})$.

determined to be 90.3% and 9.7%, respectively, calculated from the areas under the fitted curves of the allyl $+Cl(^2P_{3/2})P(E_T)$.

B. Chlorine atom angular distributions

The use of a linearly polarized laser to photolyze allyl chloride molecule and probe the $Cl(^2P_J;J=1/2,3/2)$ atomic fragment with the same laser beam yield the product recoil angular distributions shown in Figs. 3 and 4. The $Cl(^2P_{1/2})$ angular distribution (Fig. 4) is fit using the following expression:[11]

$$I(\theta)\propto 1+\beta P_2(\cos\theta), \tag{1}$$

where θ is the angle between the product recoil velocity and the polarization axis of the photolysis laser. $I(\theta)$ is the integrated signal over a certain speed range at angle θ and $P_2(\cos\theta)$ is the second-order Legendre polynomial. An anisotropy parameter β of 0.06 ± 0.01 is obtained for $Cl(^2P_{1/2})$ with the signal integrated over the speed range of 1700~2400 m/s, indicating a nearly isotropic distribution. The angular distribution for the ground state chlorine (Fig. 3), however, cannot be fit by the above equation. The $Cl(^2P_{3/2})$ atoms, having $J>1/2$, may have an aligned m_J distribution that can influence the efficiency of the linearly polarized REMPI process.[12–15] The detected $Cl(^2P_{3/2})$ angular distribution in Fig. 3 is thus fit by

$$I(\theta)\propto 1+\beta_2 P_2(\cos\theta)+\beta_4 P_4(\cos\theta). \tag{2}$$

Note that the coefficient β_2 in the above equation is influenced by the laboratory frame quadrupole alignment A_0 as well as the photofragment angular distribution, therefore is not equal to the spatial anisotropy parameter β in Eq. (1). The relationship is given in Eqs. (9)–(13) in Ref. 15. Thus β_2 cannot be used to characterize the product recoil anisotropy. Two different set of β_x parameters are obtained from the $Cl(^2P_{3/2})$ angular distribution: one corresponding to the low-kinetic energy component with the $Cl(^2P_{3/2})$ speed below 1335 m/s [Fig. 3(a)] and the other representing the high-kinetic energy component with the speed between 1500 and 2400 m/s [Fig. 3(b)]. The parameters are $\beta_2=0.47\pm0.02$ and $\beta_4=0.34\pm0.02$ for the low-kinetic energy component and $\beta_2=0.16\pm0.01$ and $\beta_4=0.06\pm0.01$ for the high-kinetic energy component.

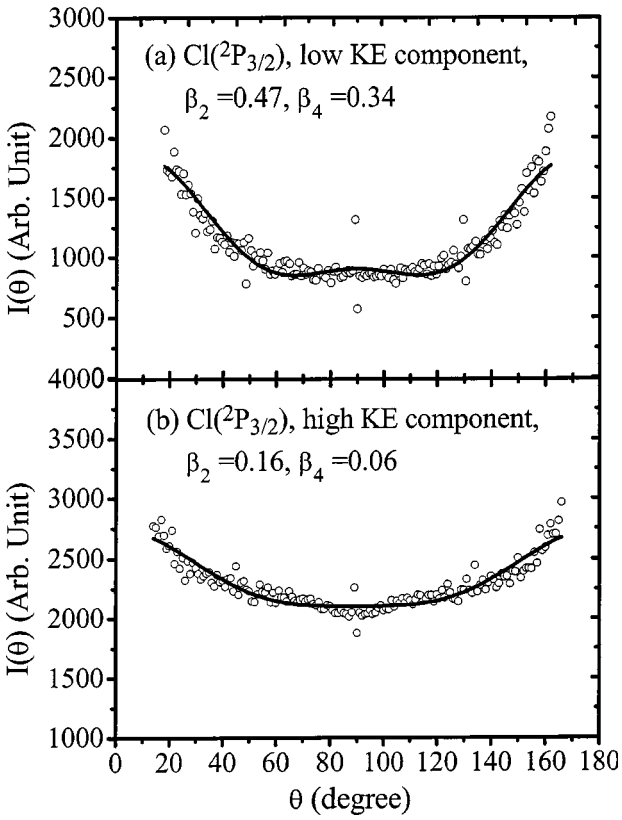

FIG. 3. Fits for $Cl(^2P_{3/2})$ fragment angular distribution: (a) low-kinetic energy component with the speed range 0–1335 m/s, $\beta_2=0.47\pm0.02$, $\beta_4=0.34\pm0.02$; (b) high-kinetic energy component with the speed range 1500–2400 m/s, $\beta_2=0.16\pm0.01$, $\beta_4=0.06\pm0.01$.

C. Spin–orbit branching ratio

REMPI detection of $Cl(^2P_{3/2})$ and $Cl(^2P_{1/2})$, respectively, allows us to determine the relative population of the fine-structure states of the fragment chlorine atoms. Since the $Cl(^2P_{3/2})$ and $Cl(^2P_{1/2})$ atoms are probed at very similar one-color REMPI wavelengths with the same laser power, the influence of photolysis and ionization photon intensity on the spin–orbit branching ratio can be ruled out. The slight difference between photodissociation cross sections at these wavelengths can also be neglected. The relative REMPI detection efficiencies,[16–20] however, must be accounted for. Liyanage *et al.*[16] determined the relative line strength for the $4p\ ^2P_{1/2}\leftarrow 3p\ ^2P_{1/2}$ and $4p\ ^2D_{3/2}\leftarrow 3p\ ^2P_{3/2}$ transitions to be 0.85 ± 0.10. The spin–orbit branching ratio of the $Cl(^2P_{3/2})$ and $Cl(^2P_{1/2})$ products can therefore be obtained by integrating the ion signal intensity over the entire velocity range of the chlorine images, scaled by the relative line strength. The $Cl(^2P_{3/2})/Cl(^2P_{1/2})$ ion signal intensity ratio has been measured to be 1.71 ± 0.15. Therefore a value of 2.01 ± 0.17 is determined for the relative population of the $Cl(^2P_{3/2})/Cl(^2P_{1/2})$ photofragments and the resultant quantum yields are $\Phi[Cl(^2P_{3/2})]=0.668\pm0.020$ and $\Phi[Cl(^2P_{1/2})]=0.332\pm0.020$. In addition to the spin–orbit branching fraction, the Cl atom product population distributions were also subdivided according to the relative amounts of the low- and high-kinetic energy components, obtained from the fit to the $P(E_T)$'s. As a result, the branching ratio of (low-kinetic energy C–Cl fission channel):(high-kinetic energy C–Cl bond fission channel) is 0.065:0.935.

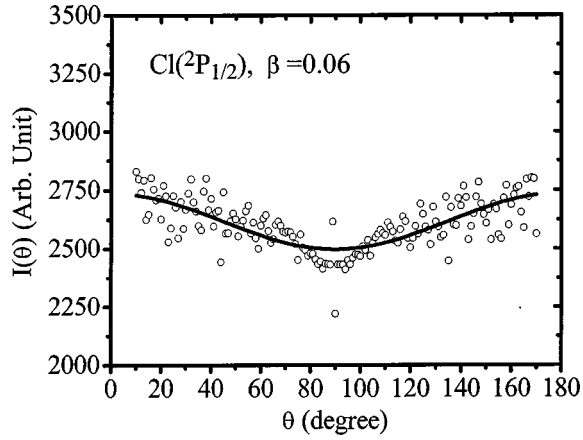

FIG. 4. Fit for $Cl(^2P_{1/2})$ fragment recoil anisotropy. Signal is integrated over the speed range of 1700–2400 m/s, $\beta=0.06\pm0.01$.

IV. DISCUSSION

Our data at 235 nm evidences a competition between a minor internal conversion channel for C–Cl bond fission, resulting in low kinetic energy $Cl(^2P_{3/2})$ products, and a dominant electronic predissociation channel that produces both $Cl(^2P_{1/2})$ products and $Cl(^2P_{3/2})$ products with high recoil kinetic energies. The kinetic energy distributions measured in this study are quite different from the one other reported study at 235 nm, by Park, Lee, and Jung.[4] We presume that study is in error as the relative contributions of the high-kinetic energy channel and the low-kinetic energy channel reported here are quite similar to those measured in molecular beam photofragmentation experiments[3] at 193 nm with tunable vacuum ultraviolet photoionization detection of the chlorine atom and its momentum-matched primary and secondary coproducts.

The peak positions of the translational energy release distributions for the C–Cl bond fission producing $Cl(^2P_{1/2})$ and the fast component of $Cl(^2P_{3/2})$ are very similar to each other (~30.0 kcal/mol). However, the distribution for $Cl(^2P_{1/2})$ is considerably narrower than that of the fast $Cl(^2P_{3/2})$. They have 8.6 and 13.0 kcal/mol FWHM, respectively. Previous photodissociation studies of allyl chloride[2,3] have identified these high-kinetic energy C–Cl bond fission channels as predissociation of the photoprepared $\pi\pi^*$ state by a nearby singlet $n\sigma^*$ state (or a $\pi\sigma^*$ state at nonplanar geometries). The repulsive nature of the potential energy surface at longer C–Cl internuclear separations thus predicts a large energy release into product recoil. The amount of kinetic energy release can be explained by a simple impulsive model.[21] There are two limiting cases of this impulsive model. The ''soft radical'' impulsive model assumes that upon initial bond rupture, momentum conservation is completely localized between the bonded carbon and chlorine atoms; energy redistribution between the recoiling C atom and the internal mode of the forming radical is achieved subsequently as the carbon collides with the other atoms in

the radical moiety. In this picture, the fraction of the available energy partitioned into product recoil is given by

$$f_{\mathrm{T,soft}}=\frac{\mu_a}{\mu_f}, \tag{3}$$

where μ_a is the reduced mass of Cl and the adjacent C atom and μ_f is the reduced mass of the allyl radical and the Cl atom. For allyl chloride, $f_{\mathrm{T,soft}}$ is calculated to be 0.47. It must be pointed out that $f_{\mathrm{T,soft}}$ obtained from the soft radical model is the lower limit for the fraction of translational energy release assuming an impulsive recoil. Another ''rigid radical'' model postulates that during the C–Cl bond fission process, the allyl radical remains rigid with no internal vibrations excited. A repulsive kick provided by the recoiling Cl atom at the end carbon atom generates rotational energy in the forming allyl radical fragment. In this model, the fraction of energy released as translation is

$$f_{\mathrm{T,rigid}}=\frac{I}{I+\mu_f r_{\mathrm{cm}}^2 \sin^2\chi}, \tag{4}$$

where $r_{\mathrm{cm}}=|\vec{r}_{\mathrm{cm}}|$, $\vec{r}_{\mathrm{cm}}$ is the vector from the alpha carbon to the allyl radical moiety's center of mass in the molecule; I is the moment of inertia of the allyl radical moiety about an axis perpendicular to the plane defined by the C–Cl bond and $\vec{r}_{\mathrm{cm}}$, and χ is the angle between the C–Cl bond and $\vec{r}_{\mathrm{cm}}$. There are two conformers for allyl chloride: *cis* and *gauche*, with their equilibrium geometries calculated by Durig *et al.*[22] The $f_{\mathrm{T,rigid}}$ values predicted using the equilibrium geometries of the *cis* and *gauche* conformers are extremely close to each other; the rigid radical impulsive limit prediction for the fraction of the total available energy partitioned to product translation is $0.60=f_{\mathrm{T,rigid}}$. In this limit, there is no vibrational excitation of the molecular fragment, so $f_{\mathrm{T,rigid}}$ should be the upper bound for the fraction of available energy released as translational energy. The experimentally measured f_{T} at 235 nm for the channel that proceeds via electronic predissociation by a state repulsive in the C–Cl bond and produces $\mathrm{Cl}(^2P_{1/2})$ is 0.59, quite close to the prediction of the rigid radical limit. This suggests that the torque exerted on the allyl moiety at the curve crossing is similar to that predicted from the equilibrium geometry. In contrast, Morton *et al.*[3] observed an f_{T} of 0.50 at 193 nm photodissociation of allyl chloride, indicating that the fast allyl radicals produced from 193 nm photolysis are vibrationally more excited than those from 235 nm dissociation.

As discussed in Sec. III, since product alignment is incorporated into the detected angular distribution of $\mathrm{Cl}(^2P_{3/2})$, the β_x parameters cannot be directly used to characterize the nature of parent molecule excitation and dissociation. Nevertheless, the angular distribution for spin–orbit excited state chlorine can be used to determine the spatial anisotropy parameter β. The measured anisotropy parameter β for $\mathrm{Cl}(^2P_{1/2})$ equals to 0.06, suggesting a slightly parallel excitation. This is inconsistent with the result of Myers *et al.*;[2] where they observed slight perpendicular anisotropy for C–Cl bond fission with $\beta=-0.1$. The discrepancy is not surprising, however, since Myers *et al.* used a 193 nm photon to dissociate allyl chloride in their study while we used a 235 nm photon. Different excitation energies can cause variations in the direction of the electronic transition dipole moment, the geometry of the excited state molecule as it evolves toward electronic predissociation, and the predicted angular distribution for both the *cis* and *gauche* conformers. In contrast to the photodissociation of alkyl iodide at 266 nm and methyl chloride at 193 nm, where the dominant transition dipole moment lies along the C–X bond and the halogen atom product recoils with a parallel angular distribution,[21,23,24] the case of allyl chloride is more complicated due to the C=C chromophore. Emission spectroscopy of allyl chloride at 199 nm evidences an admixture of the dominant $\pi_{\mathrm{C=C}}$ character with some $\sigma^*_{\mathrm{C-Cl}}$ character in the Franck-Condon region upon electronic excitation,[25] indicating that the transition dipole moment is no longer along the C–Cl bond and dependent on the allyl chloride conformation. The anisotropy parameter can therefore be deemed to be a weighted average of the predicted β values from various conformers. Myers estimated this weighted average to be 0.0 assuming that the transition dipole moment is along the C=C bond and assuming photoexcitation of the molecule does not alter the C–Cl bond direction before dissociation and both *cis* and *gauche* conformers contribute equally to the C–Cl bond fission. A β value of zero corresponds to an isotropic angular distribution. Although this picture qualitatively interprets the low anisotropy of the product recoil in the 235 nm photodissociation of allyl chloride, it does not include the differences in the nature of the excited state for the two conformers revealed in the work by Browning *et al.*[25]

Our experiment reveals that $\mathrm{Cl}(^2P_{1/2})$ fragments are less abundant than the $\mathrm{Cl}(^2P_{3/2})$ products, with a total quantum yield of 33.2%, in good agreement with that reported by Park *et al.*[4] However, Park *et al.* observed low kinetic energy Cl atoms produced in both the $\mathrm{Cl}(^2P_{1/2})$ and $\mathrm{Cl}(^2P_{3/2})$ states while our study shows this channel only produces Cl atoms in the $\mathrm{Cl}(^2P_{3/2})$ state. We do not understand the discrepancy between the two studies, done at the same wavelength with similar methodology, so we proceed with discussing our results independent of theirs. A minor portion (6.5%) of all the C–Cl bond fission events in our study is observed to impart low translational energy into product recoil, in reasonable agreement with the findings of Morton *et al.*[3] (3%), considering the difference in excitation energy. Internal conversion from the photoprepared $\pi\pi^*$ state to the vibrationally hot ground state and subsequent bond dissociation is proposed to be responsible for this low-kinetic energy channel. The low-kinetic energy C–Cl bond fission channel produces only $\mathrm{Cl}(^2P_{3/2})$, as the electronic ground state of allyl chloride asymptotically correlates to spin–orbit ground state chlorine.

Anisotropy parameters and spin–orbit branching fractions for the resolved fine-structure states of open-shell atomic fragments from photodissociation of diatomic molecules or simple alkyl halides such as HCl and CH_3Cl can be predicted by considering the nonadiabatic transitions between the potential energy surfaces at long R–Cl distances.[17,23,26–28] For instance, in the photofragmentation of HCl within the excitation energy range of 40 000–70 000 cm^{-1}, the oscillator strength is carried primarily by the

$^1\Pi(1)$ state in the Franck-Condon region, which correlates adiabatically with the lower Cl spin–orbit state ($^2P_{3/2}$). If the C–Cl bond rupture proceeds adiabatically via the repulsive $^1\Pi(1)$ state, then one should expect to see a negligible amount of Cl($^2P_{1/2}$). Lambert, Dagdigian, and Alexander[29] have performed theoretical calculations and experimental measurements of the spin–orbit branching in the photodissociation of HCl in the above energy range. They observed a significant amount of Cl($^2P_{1/2}$) and a strong dependence of the spin–orbit branching on the photoexcitation energy. This suggests that nonadiabatic transition from the initially populated $^1\Pi(1)$ state to the nearby $^3\Sigma(1)$ state, which correlates to the excited-state channel, is also involved in the photodissociation process. Since the nonadiabatic curve crossing probability increases with the translational energy of the recoiling photofragments, one should anticipate the branching fraction for excited-state Cl to approach the statistical limit of 1/3 with increasing excitation wave number. The theory also predicts that for HCl dissociation, but not DCl, the Cl($^2P_{1/2}$) branching fraction increases from zero at a low excitation energy (the threshold to energetically access the upper spin–orbit state of Cl) to a value above 1/3 and then regress toward 1/3. The high value at intermediate photon energy is confirmed in the experimental results in Lambert's study. (However, they use a line strength factor different from ours, that gives higher Cl($^2P_{1/2}$) yields.) Note that unlike the more familiar curve crossing process in methyl iodide, where the polyatomic analog of the $^1\Pi(1)$ and the $^3\Pi(0)$ curves determine the branching between I atom spin-orbit states in the 266 nm photodissociation, the interaction between these states in HCl/DCl is negligible.

Although allyl chloride photodissociation is not initiated on a repulsive potential energy surface, we have assumed that the $\pi\pi^*$ excited state is predissociated by a $^1n\sigma^*$(C–Cl) diabat, which is analogous to the optically bright $^1\Pi(1)$ state of HCl. However, considering the much heavier reduced mass of allyl chloride than HCl, it would be more appropriate to compare our experimental results on allyl chloride with the theoretical prediction of DCl and to extrapolate that to an even larger reduced mass. Lambert *et al.*[29] predicted a significantly smaller product branching into the upper spin–orbit state of DCl than HCl due to its lesser tendency to undergo nonadiabatic transitions with heavier reduced mass. At the photolysis wavelength of 235.3 nm (42 544 cm^{-1}), the Cl($^2P_{1/2}$) branching fraction is calculated to be about 0.13 for DCl. If the branching fraction of allyl chloride is determined in a similar manner, the $^2P_{1/2}$ state should be even less populated than that of DCl, since the nonadiabatic transition probability for allyl chloride is lower as a result of its even heavier reduced mass. In contrast, our experimentally measured branching fraction of Cl($^2P_{1/2}$)/[Cl($^2P_{1/2}$)+Cl($^2P_{3/2}$)] for allyl chloride is 0.355 for the high recoil kinetic energy channel following 235 nm photodissociation, much higher than the theoretical prediction of DCl, but somewhat close to the statistical limit of 0.33. This leads us to infer that the photodissociation of allyl chloride does not proceed in the same way as HCl/DCl. In those systems, recent time-dependent calculations[30] have suggested that the spin–orbit branching fraction is determined by a nonadiabatic transition from the repulsive $^1\Pi(1)$ adiabat to the $^3\Sigma^+(1)$ potential energy surface starting at an internuclear distance of around 4 bohrs and a subsequent transfer of flux to the $^3\Pi(1)$ adiabat in the region of 6–8 bohrs (see Fig. 5). In allyl chloride, however, we infer that the angular momentum recoupling[26–28] that results in transition between potential energy surfaces correlating to the allyl+Cl($^2P_{1/2}$) and allyl+Cl($^2P_{3/2}$) asymptotes occurs in the region where the energy difference is comparable to the Cl($^2P_{3/2}$)/Cl($^2P_{1/2}$) spin–orbit splitting, therefore giving a nearly statistical Cl($^2P_{1/2}$) branching fraction of 0.355 for the high recoil kinetic energy channel in the 235 nm photodissociation of allyl chloride. This is consistent with our observation of very similar kinetic energy distributions for the Cl($^2P_{1/2}$) and Cl($^2P_{3/2}$) products in the high recoil kinetic energy channel, both peaking at 30 kcal/mol, since the kinetic energy release has been largely determined at the stage when the spin–orbit recoupling occurs.

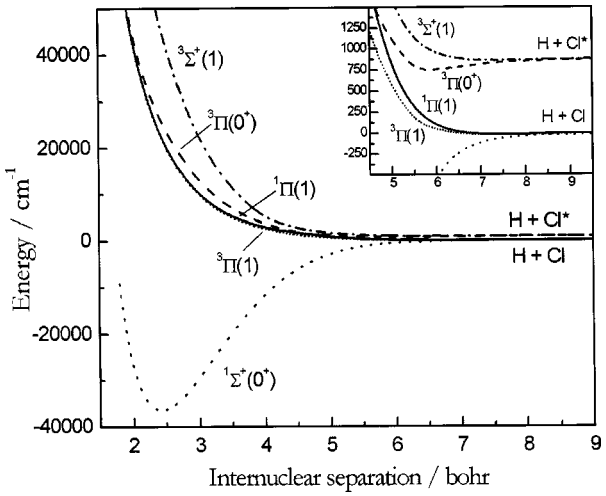

FIG. 5. Plot of the adiabatic potential energy curves of HCl used in the time-dependent calculations in Ref. 25. The inset shows an expanded view of the long-range parts of the potentials. The different curves are $X\,^1\Sigma^+(0^+)$ (- - -); $^3\Pi(1)$ (· · · · ·); $^1\Pi(1)$ (——); $^3\Pi(0^+)$ (— — —); $^3\Sigma^+(1)$ (-·-·-·-). Reproduced from Fig. 1 in Ref. 30 with permission, American Institute of Physics, Copyright 2000.

ACKNOWLEDGMENTS

This work was supported by the Chemical, Geosciences and Biosciences Division, Office of Basic Energy Sciences, Office of Science, U.S. Department of Energy, under Grant No. DE-FG02-92ER14305.

[1] J. A. Mueller, B. F. Parsons, L. J. Butler, F. Qi, O. Sorkhabi, and A. G. Suits, J. Chem. Phys. **114**, 4505 (2001).
[2] T. L. Myers, D. C. Kitchen, B. Hu, and L. J. Butler, J. Chem. Phys. **104**, 5446 (1996).
[3] M. L. Morton, L. J. Butler, T. A. Stephenson, and F. Qi, J. Chem. Phys. **116**, 2763 (2002).
[4] M. S. Park, K. W. Lee, and K. H. Jung, J. Chem. Phys. **114**, 10368 (2001).
[5] A. J. R. Heck and D. W. Chandler, Annu. Rev. Phys. Chem. **46**, 335 (1995).
[6] A. T. J. B. Eppink and D. H. Parker, Rev. Sci. Instrum. **68**, 3477 (1997).
[7] Y. Sato, Y. Matsumi, M. Kawasaki, K. Tsukiyama, and R. Bersohn, J. Phys. Chem. **99**, 16307 (1995).
[8] S. Arepalli, N. Presser, D. Robie, and R. J. Gordon, Chem. Phys. Lett. **118**, 88 (1985).

[9] J. A. Streitwieser and C. H. Heathcock, *Introduction to Organic Chemistry*, 3rd ed. (Macmillan, New York, 1985).
[10] V. Dribinski, A. Ossadtchi, V. A. Mandelshtam, and H. Reisler, Rev. Sci. Instrum. **73**, 2634 (2002).
[11] R. N. Zare, Mol. Photochem. **4**, 1 (1972).
[12] T. P. Rakitzis and R. N. Zare, J. Chem. Phys. **110**, 3341 (1999).
[13] T. P. Rakitzis, S. A. Kandel, A. J. Alexander, Z. H. Kim, and R. N. Zare, J. Chem. Phys. **110**, 3351 (1999).
[14] M. J. Bass, M. Brouard, A. P. Clark, C. Vallance, and B. Martinez-Haya, Phys. Chem. Chem. Phys. **5**, 856 (2003).
[15] P. C. Samartzis, B. L. G. Bakker, T. P. Rakitzis, D. H. Parker, and T. N. Kitsopoulos, J. Chem. Phys. **110**, 5201 (1999).
[16] R. Liyanage, Y. A. Yang, S. Hashimoto, R. J. Gordon, and R. W. Field, J. Chem. Phys. **103**, 6811 (1995).
[17] Y. Matsumi, P. K. Das, M. Kawasaki, K. Tonokura, T. Ibuki, G. Inoue, S. Satyapal, and R. Bersohn, J. Chem. Phys. **97**, 5261 (1992).
[18] V. Skorokhodov, Y. Sato, K. Sato, Y. Matsumi, and M. Kawasaki, J. Phys. Chem. **100**, 12321 (1996).
[19] M. Ahmed, D. Blunt, D. Chen, and A. G. Suits, J. Chem. Phys. **106**, 7617 (1997).
[20] J. Zhang, M. Dulligan, and C. Wittig, J. Chem. Phys. **107**, 1403 (1997).
[21] S. J. Riley and K. R. Wilson, Bull. Am. Phys. Soc. **17**, 110 (1972).
[22] J. R. Durig, D. T. Durig, M. R. Jalilian, M. Z. Zhen, and T. S. Little, J. Mol. Struct. **194**, 259 (1989).
[23] Y. Matsumi, P. K. Das, and M. Kawasaki, J. Chem. Phys. **92**, 1696 (1990).
[24] M. Kawasaki, K. Suto, Y. Sato, and Y. Matsumi, J. Phys. Chem. **100**, 19853 (1996).
[25] P. W. Browning, D. C. Kitchen, M. F. Arendt, and L. J. Butler, J. Phys. Chem. **100**, 7765 (1996).
[26] Y. B. Band, K. F. Freed, S. J. Singer, and C. J. Williams, J. Phys. Chem. **91**, 5402 (1987).
[27] S. J. Singer, K. F. Freed, and Y. B. Band, Adv. Chem. Phys. **61**, 1 (1985).
[28] S. J. Singer, K. F. Freed, and Y. B. Band, J. Chem. Phys. **79**, 6060 (1983).
[29] H. M. Lambert, P. J. Dagdigian, and M. H. Alexander, J. Chem. Phys. **108**, 4460 (1998).
[30] P. M. Regan, D. Ascenzi, A. Brown, G. G. Balint-Kurti, and A. J. Orr-Ewing, J. Chem. Phys. **112**, 10259 (2000).